J Ther Eng, Vol. 10, No. 1, pp. 88−100, January, 2024

Journal of Thermal Engineering
Web page info: https://jten.yildiz.edu.tr
DOI: 10.18186/thermal.1429382

Research Article

Brownian motion models effect on the nanofluid fluid flow and heat transfer in the natural, mixed, and forced convection

Behrooz MOZAFARY[1,*], Ali AKBAR[1], Abbasian ARANI[1], Ghanbar Ali SHEIKHZADEH NOOSHABADI[2], Mohammad SALIMI[3]

[1]*Department of Mechanics, Energy Conversion, Islamic Azad University, Arak Branch, Arak, 1477893855, Iran*
[2]*Department of Mechanical Engineering, Faculty of Heat and Fluid, University of Kashan, Kashan, Iran, and Islamic Azad University, Arak Branch, Arak, 1477893855, Iran*
[3]*Department of Chemical Engineering, Islamic Azad University, Arak Branch, Arak, 1477893855, Iran*

ARTICLE INFO

Article history
Received: 18 May 2021
Accepted: 27 July 2021

Keywords:
Nanofluid; Brownian Motion; Numerical Solution; Variable Properties; Natural Convection; Mixed Convection; Forced Convection

ABSTRACT

In this research, the effect of different models of thermal conductivity and dynamic viscosity has been investigated by considering the effect of Brownian motion of nanoparticles on the flow field and heat transfer of nanofluids. This study was performed numerically in a square cavity with water/aluminum-oxide nanofluid in three modes of natural, mixed and forced convection by changing the independent variable such as nanoparticle volume fraction, Rayleigh number, Richardson number, and Reynolds number. The governing equations with certain boundary conditions are solved using the finite volume method. Also, according to the obtained numerical results, Nusselt number has been investigated for different conditions with and without considering Brownian motion. The results showed that for all the studied models, in all three modes of natural, mixed and forced convection, the average Nusselt number when the effect of Brownian motion is considered, is more than the case that the effect of this motion is not considered. In all cases, the Koo & Kleinstreuer and Li & Kleinstreuer models show approximately the same values for the maximum mean Nusselt number. The similar results are obtained employing the Wajjha & Das and Xiao et al. models. For mixed convection, the highest and lowest increases of Nusselt number, considering Brownian motion are 17.68% and 14.84%, respectively. While referred values for forced convection are 30.46% and 17.94 %, respectively.

Cite this article as: Mozafary B, Akbar A, Arani A, Sheikhzadeh Nooshabadi GA, Salimi M. Brownian motion models effect on the nanofluid fluid flow and heat transfer in the natural, mixed, and forced convection. J Ther Eng 2024;10(1):88−100.

INTRODUCTION

One of the methods to increase the heat transfer is to use fluids that are composed of mixing common fluids such as water, Ethylene Glycol, oil as the base fluid, and solid particles of nanometer dimensions. In the recent years, nanofluids and their relevant phenomena have drawn much attention. The use of nanofluids as a passive method in heat

***Corresponding author.**
*E-mail address: mozafaryb@yahoo.com

This paper was recommended for publication in revised form by Mustafa Kılıç

Published by Yıldız Technical University Press, İstanbul, Turkey

transfer has been focused many attention [1-4]. For example, Rajesh et al. [5] examined the transient magnetohydrodynamics (MHD) flow and heat transfer of the nanofluid due to vertical plate motion by considering the radiation effect, the oscillating temperature effect, and Brownian motion. They studied the free convection heat transfer for a viscous, electrically conductive, and incompressible nanofluid following over a semi-infinite vertical plate. The nanofluid used was a water/copper nanofluid. They presented their obtained results as velocity distribution, temperature field, and Nusselt number variation. The results of this study demonstrated the important factors that affecting the fluid flow and heat transfer. Shahriari et al. [6] examined the effect of independent variables as temperature, average nanoparticle size, and nanoparticle concentration on the dynamic viscosity of the nanofluid, relying on an analytical method of modified equations of nanofluid viscosity. The new model developed from the previous models that considered the effect of Brownian motion as a key parameter. Sepehrnia et al. [7] examined the flow field and heat transfer of water/aluminum-oxide nanofluid in a rectangular microchannel, consisting of seven microchannels with equilaterally triangular cross-section in numerical and three-dimensional forms considering conductive solid parts. The governing equations were solved via the finite volume method using the SIMPLE algorithm. The goal was to examine the effect of four different configuration on the flow field and heat transfer of water/aluminum-oxide nanofluid. They used from nanofluids and an increase in the volume fraction from 0 to 4% resulted in increasing the average Nusselt number from 4.72% to 5.47%, reduced the thermal resistance from 2.34% to 1.81%, and reduced the maximum ratio of the temperature difference of the wall to the heat flux from 1.56% to 1.28%. Khorasanizadeh et al. [8] also investigated the smooth flow of nanofluid, heat transfer, and other functional properties of a wall, consisting of seven microchannels with a three-dimension equilaterally triangular cross-section by considering the conductive solid parts. Here, a horizontal inlet and outlet array (I-type configuration) and a vertical inlet and outlet type (U-type configuration) were considered, and a constant inlet heat flux of 125 kW/m^2 to the wall was simulated. Their findings suggested that for both considered configurations, the pressure drop increases, the thermal performance improves in terms of heat transfer, thermal resistance, and uniform distribution of temperature at the floor. In another study, Rajesh et al. [9] examined the transient MHD free convection flow field and heat transfer of nanofluid from vertical plate motion in the presence of temperature-dependent viscosity by taking into account the effects of Brownian motion. They used finite element and the Galerkin methods to develop a mathematical model to solve the governing equations. This study demonstrates that the velocity and temperature profiles as well as the coefficient of friction and Nusselt number were changed considerably due to considering the Brownian motion in nanofluid thermal conductivity estimation. The independent parameters are included: Grashof number, type of nanoparticle, nanoparticle volume fraction, magnetic parameters, Eckert number, and suction parameters. Seth and Mishra [10] investigated the transient MHD nanofluid flow passing through a nonlinear plate considering the Navier's slip boundary condition and the effects of Brownian motion of particles. In their study, they considered the effect of radiation heat transfer and magnetic field. They developed a finite element mathematical model via the Glerkin method to perform numerical simulations. They also examined the changes in such parameters as Nusselt number, surface friction coefficient, and Sherwood number in terms of different variables. Aghabzorg et al. [11] experimentally examined the improved heat transfer of magnetic iron oxide nanoparticles of water-MWCNT for smooth and transient turbulence in a plate heat exchanger considering the effects of particles Brownian motion. They demonstrated the changes in convective heat transfer coefficient in terms of Reynolds number and volume fraction. Fan et al. [12] experimentally examined the effect of the aqueous graphene nanofluids concentration on the transient heat transfer of the boiling pool by considering the effects of the Brownian motion of the particles. This was performed by placing stainless steel spheres in dilute aqueous nanofluids containing grapheme-oxide nanosheets (GONs) in various volume fractions up to 0.1%. They reported their findings for thermal temperature and flux in terms of superheat temperature, the temperature in terms of time, and contact angle in terms of nanosheet concentration. Suganthi et al. [13] experimentally investigated the transient convective heat transfer properties of zinc oxide nanofluids in ethylene-glycol and ethylene-glycol/water-based refrigerants by considering the effects of particle Brownian motion. This study was carried out to enhance the thermodynamic properties of these nanofluids. Lee et al. [14] also experimentally examined the thermophysical parameters and transient natural convection of zinc-oxide Ethylene Glycol/water nanofluid, and calculated its thermal conductivity and dynamic viscosity by taking into account the effects of the Brownian motion of a particle.

Understanding the flow behavior and particle convection in nanofluids is highly important to serve as a suitable heat transfer medium. The flow behavior in such fluids can be affected by particle convection from the disproportionate distribution of concentration in the nanofluids. The conflicting findings reported by researchers over the performance of nanofluids in heat transfer can confirm this subject. Goswami et al. [15] present an analyze on mixed convection flow features of a water/CuO nanoliquid within a partially heated wavy enclosure in order to investigate the effect of Brownian motion on fluid flow and heat transfer. Employed viscosity and the thermal conductivity are depended to the Brownian motion. Harish and Sivakumar [16] provided a study on opposing and assisting mixed convection flows and heat transfer performance of nanofluids inside a cubical enclosure. It shown that the average heat transfer rate increases with decrease in Richardson number and increase in nanoparticles volume fraction for both opposing and assisting flows. The effects of Brownian motion more significant in assisting flows than opposing flows. There are a number of investigation that present the effect of Brownian motion on the fluid flow and heat transfer [17-23]. Recently, Mbugua Mburu et al. [24] present an investigation about entropy generation on OLDROYD-B nanofluid past a Riga plate. They study the effect of various parameters as Brinkman number, Prantl number and the Brownian motion parameter on fluid flow and entropy generation. In another investigation Makkar et al. [25] present a study on Casson nanofluid flow toward a non-linear sheet. They study the effect of major parameters as slip velocity, thermophoresis, Brownian motion on fluid flow and heat transfer. They noticed that the Brownian motion has a major effect on the profile of nanoparticle concentration.

To model the thermal conductivity and viscosity of nanofluid coefficients, there is abundant data about the intra-structural properties of the nanofluid [24-30]. Since these properties are not fully known, researchers have only considered the effect of one of these properties to model the effects. Therefore, there are many models available to estimate the thermal conductivity and dynamic viscosity of nanofluids coefficients, the accuracy of which requires experimental results. As stated, the present study aimed to investigate the effect of different models of the Brownian motion of particles on Nusselt number in natural, mixed, and forced convection of nanofluids. In current investigation four model of thermal conductivity consisting Maxwell [31], Koo & Kleinstreuer [31] and Li & Kleinstreuer [32], Wajjha & Das [33] and Xiao et al. [34] and four model of dynamic viscosity consisting Brinkman, Koo & Kleinstreuer [31] and Li & Kleinstreuer [32], Wajjha & Das [33] and Xiao et al. [34] are employed and obtained Nusselt number are compared.

MATERIALS AND METHODS

Governing Equation

The following hypotheses were stated using the governing differential equations:

1) Newtonian fluid was considered.
2) Nanoparticles were uniform in terms of shape and size.
3) The base fluid and nanoparticles were in thermal equilibrium.
4) The presence of chemical reaction and viscous dissipation were discarded.

The system of governing equations are as follows:

$$\frac{\partial(\rho_{nf}u)}{\partial x}+\frac{\partial(\rho_{nf}v)}{\partial y}=0 \tag{1}$$

$$\frac{\partial}{\partial x}\left(\rho_{nf}uu\right)+\frac{\partial}{\partial y}\left(\rho_{nf}vu\right)=-\frac{\partial p}{\partial x}+\frac{\partial}{\partial x}\left(\mu_{nf}\frac{\partial u}{\partial x}\right)+\frac{\partial}{\partial y}\left(\mu_{nf}\frac{\partial u}{\partial y}\right) \tag{2}$$

$$\frac{\partial}{\partial x}\left(\rho_{nf}vu\right)+\frac{\partial}{\partial y}\left(\rho_{nf}vv\right)=-\frac{\partial p}{\partial y}+\frac{\partial}{\partial x}\left(\mu_{nf}\frac{\partial v}{\partial x}\right)+\frac{\partial}{\partial y}\left(\mu_{nf}\frac{\partial v}{\partial y}\right)+g(T-T_c)(\rho_{nf}\beta_{nf}) \tag{3}$$

$$\frac{\partial}{\partial x}\left(\rho_{nf}c_{nf}uT\right)+\frac{\partial}{\partial y}\left(\rho_{nf}c_{nf}vT\right)=\frac{\partial}{\partial x}\left(k_{nf}\frac{\partial T}{\partial x}\right)+\frac{\partial}{\partial y}\left(k_{nf}\frac{\partial T}{\partial y}\right) \tag{4}$$

In used system of equation, u and v refer to velocity components. T and p refer to the temperature and pressure, respectively. In addition, g and c refer to the gravity and constant specific heat capacity, respectively. k and μ refer to the thermal conductivity and dynamic viscosity, respectively. β refers to thermal expansion factor. nf refers to the nanofluid.

Density, thermal expansion factor, and constant pressure specific heat capacity are estimated by the following relations [35]:

$$\begin{gathered}\rho_{nf}=1001.064+2738.6191\varphi-0.2095T\\ 5\le T\le 40\,℃,\ \ 0\le\varphi\le 4\%\end{gathered} \tag{5}$$

$$\begin{gathered}\beta_{nf}=(-0.479\varphi+9.3158\times10^{-3}T-\tfrac{4.7211}{T^2})\times10^{-3}\\ 10\le T\le 40\,℃,\ \ 0\le\varphi\le 4\%\end{gathered} \tag{6}$$

$$c_{nf}=(1-\varphi)c_f+\varphi c_p \tag{7}$$

Non-dimensional Form of Governing Equation

Natural Convection

$$\frac{\partial(\rho^*U)}{\partial X}+\frac{\partial(\rho^*V)}{\partial Y} \tag{8}$$

$$\frac{\partial}{\partial X}(\rho^*UU)+\frac{\partial}{\partial Y}(\rho^*VU)=-\frac{\partial P}{\partial X}+Pr\left(\frac{\partial}{\partial X}\left(\mu^*\frac{\partial U}{\partial X}\right)+\frac{\partial}{\partial Y}\left(\mu^*\frac{\partial U}{\partial Y}\right)\right) \tag{9}$$

$$\frac{\partial}{\partial X}(\rho^*VU)+\frac{\partial}{\partial Y}(\rho^*VV)=-\frac{\partial P}{\partial Y}+Pr\left(\frac{\partial}{\partial X}\left(\mu^*\frac{\partial V}{\partial X}\right)+\frac{\partial}{\partial Y}\left(\mu^*\frac{\partial V}{\partial Y}\right)\right)+Ra.Pr.\rho^*.\beta^*.\theta.\cos\alpha \tag{10}$$

$$\frac{\partial}{\partial X}(\rho^*c^*U\theta)+\frac{\partial}{\partial Y}(\rho^*c^*V\theta)=\frac{1}{Re.Pr}\left(\frac{\partial}{\partial X}\left(k^*\frac{\partial\theta}{\partial X}\right)+\frac{\partial}{\partial Y}\left(k^*\frac{\partial\theta}{\partial Y}\right)\right) \tag{11}$$

In above equation non-dimensional numbers are as follows:

$$X=\frac{x}{H}\quad Y=\frac{y}{H}\quad U=\frac{uH}{\alpha_{f,o}}\quad V=\frac{vH}{\alpha_{f,o}}\quad \theta=\frac{T-T_c}{T_h-T_c}\quad P=\frac{pH^2}{\rho_{f,o}\alpha_{f,o}^2} \tag{12}$$

Force and mixed convection

$$\frac{\partial(\rho^*U)}{\partial X}+\frac{\partial(\rho^*V)}{\partial Y} \tag{13}$$

$$\frac{\partial}{\partial X}(\rho^* UU)+\frac{\partial}{\partial Y}(\rho^* VU)=-\frac{\partial P}{\partial X}+\frac{1}{Re}\left(\frac{\partial}{\partial X}\left(\mu^*\frac{\partial U}{\partial X}\right)+\frac{\partial}{\partial Y}\left(\mu^*\frac{\partial U}{\partial Y}\right)\right) \quad (14)$$

$$\frac{\partial}{\partial X}(\rho^* VU)+\frac{\partial}{\partial Y}(\rho^* VV)=-\frac{\partial P}{\partial Y}+\frac{1}{Re}\left(\frac{\partial}{\partial X}\left(\mu^*\frac{\partial V}{\partial X}\right)+\frac{\partial}{\partial Y}\left(\mu^*\frac{\partial V}{\partial Y}\right)\right) \quad (15)$$

$$\frac{\partial}{\partial X}(\rho^* c^* U\theta)+\frac{\partial}{\partial Y}(\rho^* c^* V\theta)=\frac{1}{Re.Pr}\left(\frac{\partial}{\partial X}\left(k^*\frac{\partial \theta}{\partial X}\right)+\frac{\partial}{\partial Y}\left(k^*\frac{\partial \theta}{\partial Y}\right)\right) \quad (16)$$

In above equation non-dimensional numbers are as follows:

$$X=\frac{x}{H} \quad Y=\frac{y}{H} \quad U=\frac{u}{U_0} \quad V=\frac{v}{U_0} \quad \theta=\frac{T-T_c}{T_h-T_c} \quad P=\frac{p}{\rho_{f,o}U_0^2} \quad (17)$$

It should be noted that the base fluid properties at 25 °C are used to nano-dimensional processing of the nanofluid properties:

$$\rho^*=\frac{\rho_{nf}}{\rho_{f,o}} \quad \beta^*=\frac{\beta_{nf}}{\beta_{f,o}} \quad k^*=\frac{k_{nf}}{k_{f,o}} \quad \mu^*=\frac{\mu_{nf}}{\mu_{f,o}} \quad c^*=\frac{c_{nf}}{c_{f,o}} \quad (18)$$

Where $\rho_{f,o}$, $\beta_{f,o}$, $k_{f,o}$, $\mu_{f,o}$ and $c_{f,o}$ represent density, thermal expansion coefficient, thermal conductivity, dynamic viscosity, and constant pressure heat capacity, respectively. The dynamic viscosity and constant pressure specific heat capacity of the nanofluid are at the reference temperature. The thermophysical properties of the base fluid at the reference temperature are shown in Table 1.

Boundary Conditions

Natural condition

According to Figure 1, the boundary conditions of the velocity equation are determined as follows. Considering the non-slip boundary condition, the velocity on all solid walls is considered to be zero. Therefore, the value of velocity on the solid walls is equal to:

Table 1. Thermophysical Properties of water and alumina at T=25^C [38]

Properties	Base Fluid (Water)	Alumina oxid
$\rho(kg/m^3)$	1.997	*3970*
$c_p(J/kg.K)$	4179	*765*
$k(W/m.K)$	613.0	*40*
$\beta \times 10^{-5}\ (K^{-1})$	21	*0.85*
$d(nm)$	384.0	*29*

$$v=u=0 \quad (19)$$

The temperature boundary conditions on vertical walls are:

$$x=0 \qquad 0\leq y\leq H \qquad T=T_H \quad (20)$$

$$x=H \qquad 0\leq y\leq H \qquad T=T_c \quad (21)$$

The horizontal walls of the cavity are considered insulation, so the heat flux on the horizontal walls is constant and equal to zero. Therefore, the temperature boundary conditions on vertical walls are defined as:

$$x=H \qquad 0\leq y\leq H \qquad T=T_c \quad (22)$$

Mixed Convection

According to Figure 2, the boundary conditions of the velocity and temperature equation are similar to the boundary conditions for the natural convection mode.

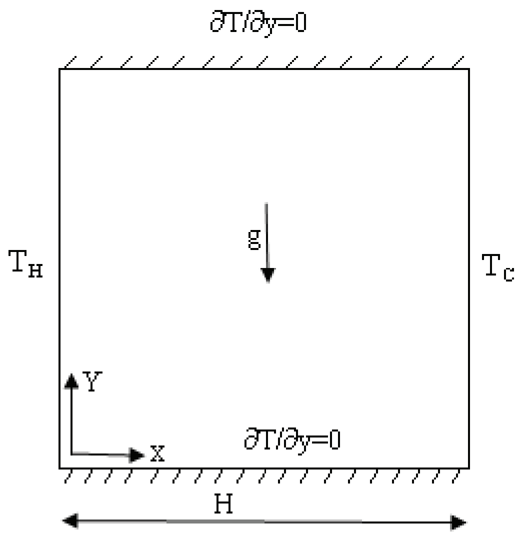

Figure 1. Schematic Diagram for natural convection.

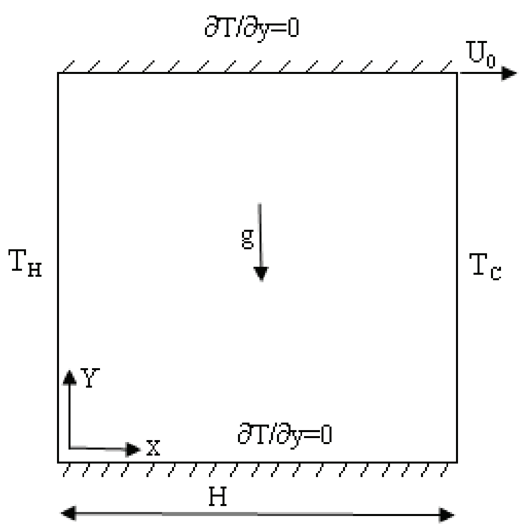

Figure 2. Schematic Diagram for mixed convection.

$$y=0,H \qquad 0\leq x\leq H \qquad \frac{\partial T}{\partial y}=0 \tag{23}$$

Forced Convection

According to Figure 3, the temperature boundary conditions of this problem are considered with the previous two cases so that the results are comparable. In this geometry, the cold flow enters from the upper part of the vertical wall on the left and the flow exits from the lower part of the vertical wall on the right. Therefore:

$$\text{Vertical right and left wall: } \begin{cases} v=u=0 \\ T=T_H \end{cases} \tag{24}$$

$$\text{Inlet flow: } \begin{cases} u=U_0 \text{ , } v=0 \\ T=T_c \end{cases} \tag{25}$$

$$\text{Outlet flow: } \begin{cases} \frac{\partial u}{\partial x}=0 \text{ , } v=0 \\ \frac{\partial T}{\partial x}=0 \end{cases} \tag{26}$$

$$\text{Horizontal up and bottom wall: } \begin{cases} v=u=0 \\ \frac{\partial T}{\partial y}=0 \end{cases} \tag{27}$$

Non-dimensional Form of Boundary Condition

Natural convection

$$Y=0,\ 0\leq X\leq 1 \rightarrow U=V=\frac{\partial \theta}{\partial Y}=0 \tag{28}$$

$$Y=1,\ 0\leq X\leq 1 \rightarrow U=V=\frac{\partial \theta}{\partial Y}=0 \tag{29}$$

$$X=0,\ 0\leq Y\leq 1 \rightarrow U=V=0,\ \theta=1 \tag{30}$$

$$X=1,\ 0\leq Y\leq 1 \rightarrow U=V=0,\ \theta=0 \tag{31}$$

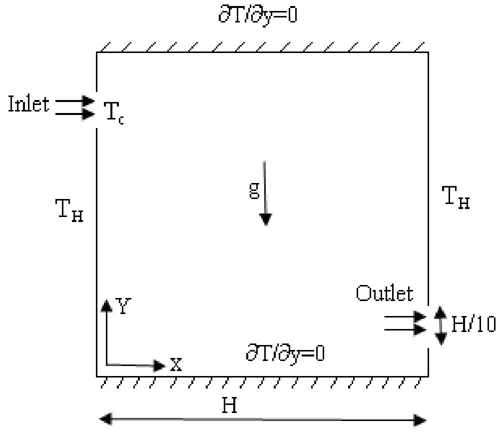

Figure 3. Schematic Diagram for forced convection.

Mixed convection

$$Y=1,\ 0\leq X\leq 1 \rightarrow U=1,\ V=\frac{\partial \theta}{\partial Y}=0 \tag{32}$$

Forced convection

$$\text{Vertical Right and left wall: } \begin{cases} V=U=0 \\ \theta=1 \end{cases} \tag{33}$$

$$\text{Inlet flow: } \begin{cases} U=1 \text{ , } V=0 \\ \theta=0 \end{cases} \tag{34}$$

$$\text{Outlet flow: } \begin{cases} \frac{\partial U}{\partial X}=0 \text{ , } V=0 \\ \frac{\partial \theta}{\partial X}=0 \end{cases} \tag{35}$$

$$\text{Horizontal up and bottom wall: } \begin{cases} V=U=0 \\ \frac{\partial \theta}{\partial Y}=0 \end{cases} \tag{36}$$

Validation

In order to validate the results of the prepared computer program, two numerical simulations are performed, one for

Table 2. Validation, comparison between the obtained results with a reference for natural convection (left Table) and a reference for mixed convection (right Table)

Ra	"φ"	Nuavg" Present Result	Nuavg" Ref. [39]	Diff.%	Ra	"φ"	Nuavg" Present Result	Nuavg" Ref. [39]	Diff.%
	0	3.34	3.37	0.89		0	32.33	32.39	0.19
10^3	02.0	3.75	3.78	0.79	0.001	0.05	34.35	34.42	0.20
	04.0	3.90	3.92	0.51		0.1	36.40	36.90	1.36
	0	3.40	3.43	0.87		0	4.62	4.73	2.33
10^4	02.0	3.81	3.84	0.78	1	0.05	4.71	4.83	2.48
	04.0	3.96	3.99	0.75		0.1	4.79	4.94	3.04
	0	4.06	4.07	0.25		0	1.63	1.68	2.98
10^5	02.0	4.46	4.48	0.45	10	0.05	1.75	1.82	3.85
	04.0	4.60	4.61	0.22		0.1	1.87	1.95	4.10
	0	5.31	5.35	0.75					
10^6	02.0	5.81	5.85	0.68					
	04.0	5.97	6.02	1.00					

natural convection and the other for mixed convection, and the results are compared with the results presented in the research [37,38], respectively. These results are presented in Tables 2. As can be seen, the relative differences in Nusselt values are very small and therefore the accuracy of the modeling results is ensured.

Grid Independence Study

To solve the problem, an N × N grid is selected to use in the solution of flow field and heat transfer and to check the independence of the results with used grid. The calculation results are obtained and compared for different N values, as presented in Table 3. Also, for more accurate results and due to the strong temperature gradients of the left and right walls for the natural convection case, the extreme temperature gradients of the left and right walls and the high wall velocity gradient for the mixed convection case and the temperature and velocity gradients of the left and right walls for the forced convection, employed grid is considered non-uniform so that the grid size is smaller around the walls where there is a temperature and velocity gradient.

Table 3. Grid independence study for natural convection case

Flow function	Average Nusselt number	Grid number
15.0669	5.9414	71×71
15.0428	5.9275	81×81
15.0249	5.9177	91×91
15.0108	5.9103	101×101
15.9995	5.9046	111×111
15.9918	5.9032	121×121
1509950	5.9011	131×131

In this section the result obtained for natural convection is reported.

RESULTS AND DISCUSSION

Thermal Conductivity Coefficient Ratio and Dynamic Viscosity Ration Variation

In this section, different models of thermal conductivity and viscosity selected in the present investigation are compared. These models include Maxwell, Koo & Kleinstreuer [31] and Li & Kleinstreuer [32], Wajjha & Das [33] and Xiao et al. [34]. Figure 4. shows the changes in the ratio of the thermal conductivity of the nanofluid to the thermal conductivity of the base fluid and the changes in the ratio of the viscosity of the nanofluid to the viscosity of the base fluid with volume fraction for different models. As can be seen from the Figure 4, the thermal conductivity and viscosity of the nanofluid increase with increasing volumetric percentage of aluminum-oxide nanoparticles. The thermal conductivity and dynamic viscosity of the nanofluid increase linearly for the Maxwell model with increasing volume fraction and nonlinearly for the other models. The increase in thermal conductivity and nanofluid viscosity for Brownian models is greater than the Maxwell model and the largest increase is related to the Brownie Koo & Kleinstreuer [31] model.

Natural convection

In the first case, the flow and heat transfer of natural convection for a range of Ra and "φ" values in 100 mm square cavities are investigated. Water was selected as the base fluid with Pr=2.6 for the present study. The cavity is filled with a mixture of water/aluminum-oxide with a diameter of 29 nm. The left wall is assumed to be hot, the

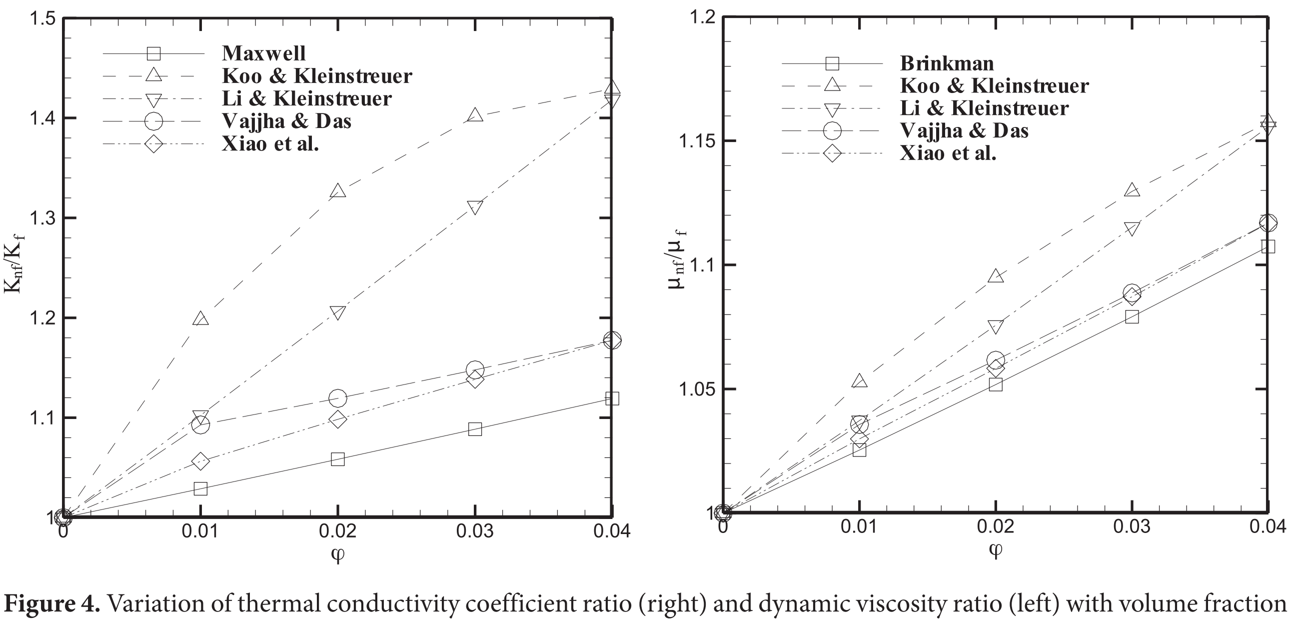

Figure 4. Variation of thermal conductivity coefficient ratio (right) and dynamic viscosity ratio (left) with volume fraction

right wall to be cold, and the top and bottom walls to be insulated. Results for Ra = 10^6-10^3, values of φ equal to 4%, 3%, % 2, and 0 and diameters of 29, 47 and 65 mm were presented once considering the effect of Brownian motion and again without considering its effect.

In Figure 5, the changes of the mean Nusselt number in the natural convection in different models are compared in terms of volume fraction in different Rayleigh numbers.

In all models and in all Rayleigh numbers, the average Nusselt number increases with increasing volume fraction. In all Rayleigh numbers, the Koo & Kleinstreuer and Li & Kleinstreuer models show the largest increase in the Nusselt number with increasing volume fraction. According to what was can be show the changes in thermal conductivity coefficient, these two models show the largest increase in flow function and thermal conductivity coefficient. Therefore, the prediction of further increase of Nusselt number by these two models is justifiable. In all Rayleigh numbers in the volume fraction of 0.04, the Koo & Kleinstreuer and Li & Kleinstreuer models show almost the same values for the mean Nusselt number. This behavior is also seen in the Wajjha & Das and Xiao et al. models. In justifying this behavior, one can present similar reason as above. In addition, the Koo & Kleinstreuer and Li & Kleinstreuer, and Wajha-Das, Xiao-et al. models show the same values for the thermal conductivity. Approximate values for the maximum flow function in the Koo & Kleinstreuer and Li & Kleinstreuer, and Wajha-Das, Xiao et al. models models in all volume fractions show very close vales. According to these two reality, the behavior of the mentioned models in volume fraction of 0.04 is justifiable.

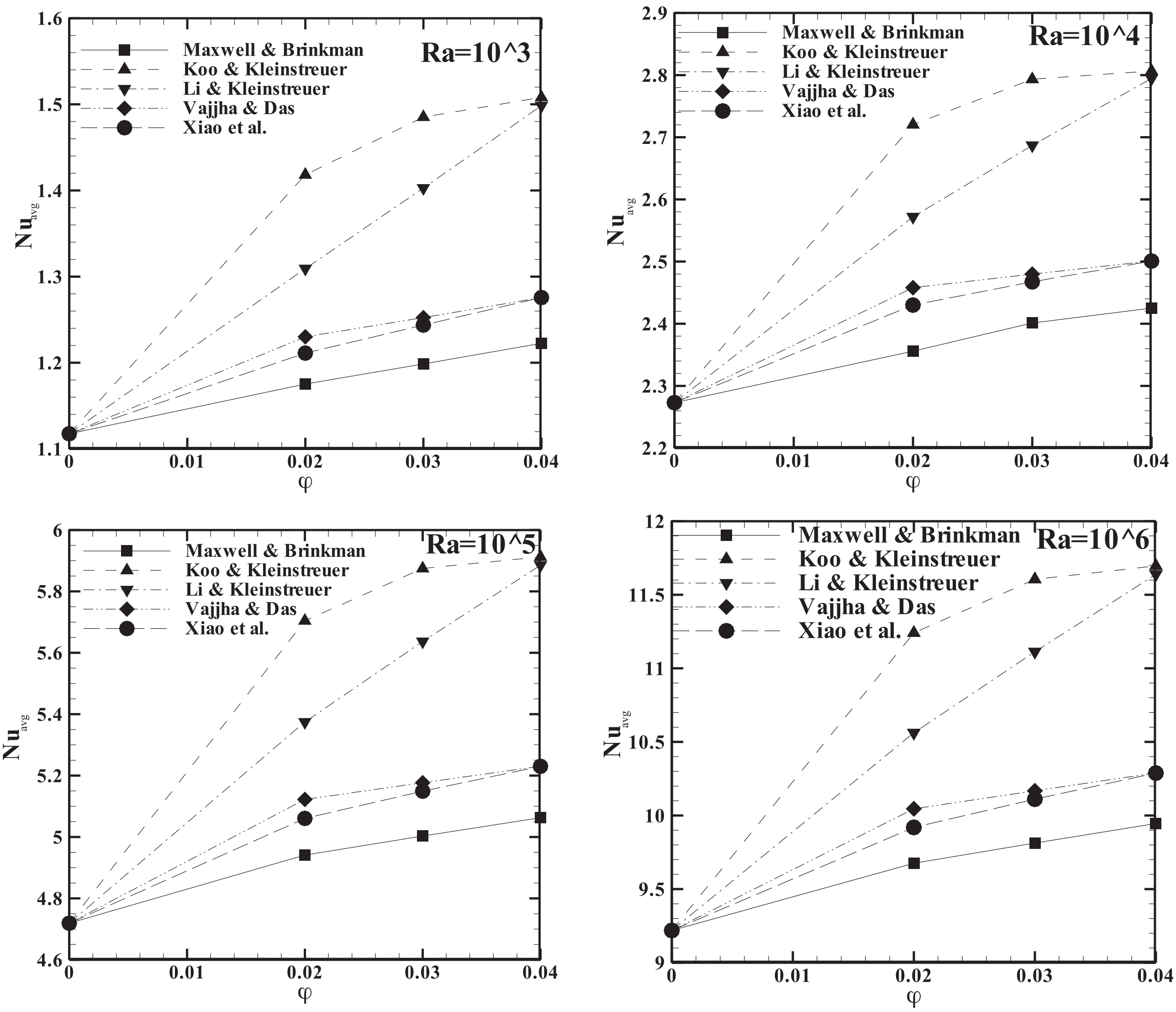

Figure 5. Average Nusselt number with volume fraction employing various thermal conductivity and dynamic viscosity in natural convection.

Mixed convection

The two-dimensional mixed convection for water/aluminum-oxide nanofluids in a square cavity with a movable cap with the same geometry as the natural convection case has been studied. The left wall is assumed to be hot, the right wall to be cold, and the top and bottom walls to be insulated. Also, the top wall moves at a constant velocity, once to the right and again to the left. Results for the fixed value of Gr= 10^4 and the range of Ri = 0.1-0.1, the values of φ equal to % 4 and% 3,% 2, 0 and nanoparticles diameters of 29, 47 and 65 mm once, taking into account the effect of Brownian motion and again without considering get the effect it provided.

In Figure 6, the mean Nusselt number changes in the mixed convection in different models are compared in terms of volume fraction in different Richardson numbers. In all

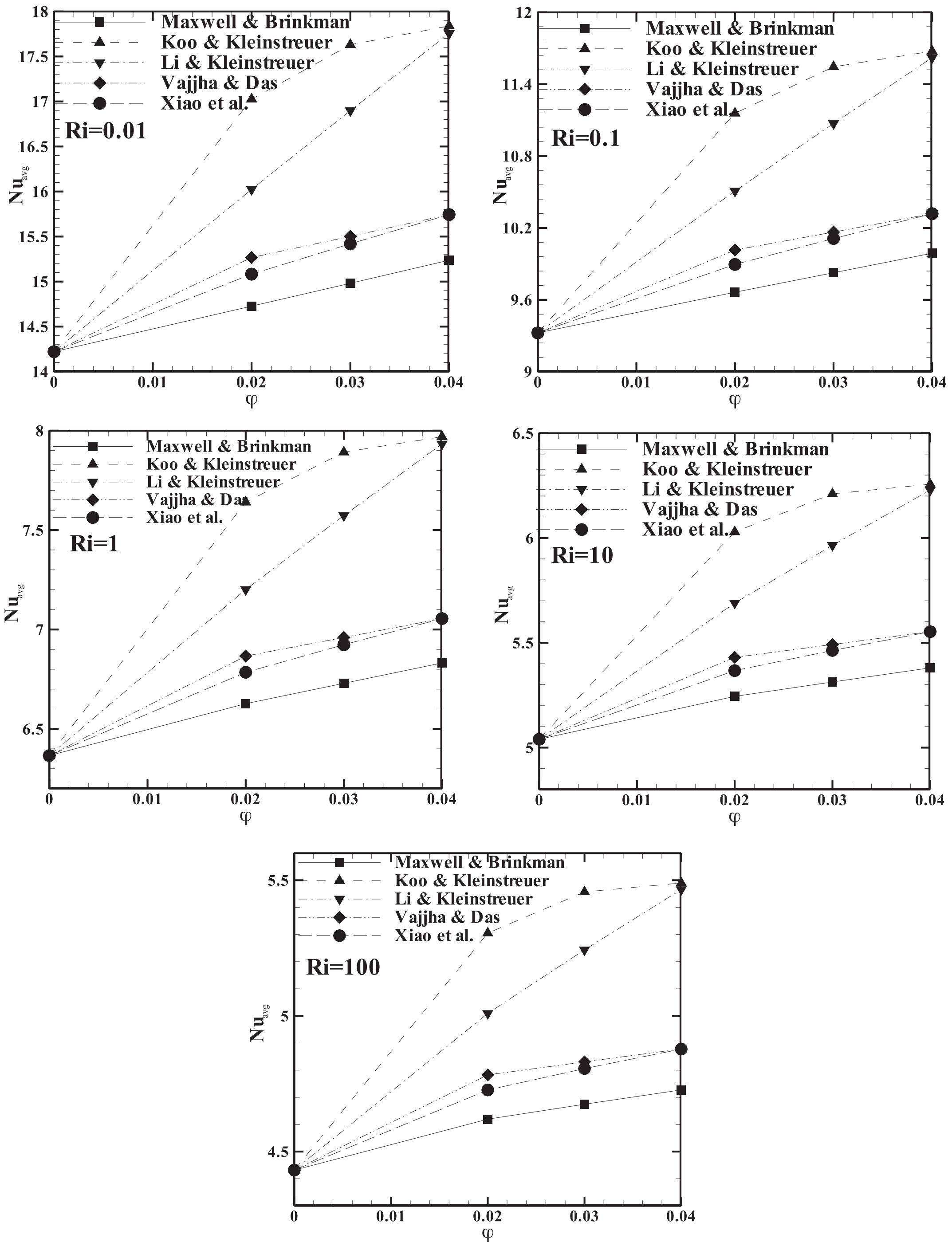

Figure 6. Average Nusselt number with volume fraction employing various thermal conductivity and dynamic viscosity in mixed convection

models and in all Richardson numbers, the mean Nusselt number increases with increasing volume fraction. For all Richardson numbers studied, the Koo & Kleinstreuer and Li & Kleinstreuer models show the largest increase in the Nusselt number with increasing volume fraction. In mixed convection, the fluid flow strength is more affected by the velocity of the cap than by the dynamic viscosity predicted by different models. This indicates that in the mixed convection, the effects of changing the thermal conductivity with the selected model are more effective than the effects of changing the viscosity.

Considering the changes in thermal conductivity are shown in Figure 4, these two models show the largest increase in thermal conductivity, so the prediction of a further increase in Nusselt number by these two models is justified. In all Rayleigh numbers in the volume fraction of 0.04, the Koo & Kleinstreuer and Li & Kleinstreuer models show the same values for the mean Nusselt number as for the natural convection mentioned in Figure 5. This behavior is also seen in the Wajjha-Das and Xiao et al. models. To justify this behavior, we can refer to Figure 4. In Figure 4, the Koo & Kleinstreuer and Li & Kleinstreuer, and Wajjha-Das, Xiao et al. models show the same values for the thermal conductivity. Very close values are observed in the maximum flow function for the Koo & Kleinstreuer and Li & Kleinstreuer, and Wajjha-Das, Xiao et al. models in all volume fractions. According to these two things, the behavior of the mentioned models in volume fraction of 0.04 is justifiable.

Table 4 shows the values of the mean Nusselt number in Rayleigh numbers and the different volume fractions for the Koo & Kleinstreuer model as a sample and is compared with the Maxwell-Brinkman fixed properties model. In the Koo & Kleinstreuer model, the highest and lowest increases in the mean Nusselt number, taking into account the effect of Brownian motion relative to the state in which this motion is not considered, are 17.68% (in Richardson 0.01, volume fraction 0.03), and is 14.84% (in Richardson 100, volume fraction is 0.02), respectively.

Forced convection

In Figure 7, the variations of the mean Nusselt number in the forced convection in different models are compared in terms of volume fraction in different Reynolds numbers. In all models and in all Reynolds numbers, the average Nusselt number increases with increasing the volume fraction. For all the studied Reynolds numbers s, the Koo & Kleinstreuer and Li & Kleinstreuer models show the largest increase in the Nusselt number with increasing volume fraction. In forced convection, such as mixed convection, the strength of the fluid flow is more affected by the velocity of the flow than by the dynamic viscosity predicted by the various models. This indicates that in forced convection as well as mixed convection, the effects of changing the thermal conductivity with the selected model are more effective than the effects of changing the dynamic viscosity with selected the model. Considering the changes in thermal conductivity that are shown in Figure 4, these two models show the largest increase in thermal conductivity, so the prediction of a further increase in Nusselt number by these two models is justified. Table 5 shows the mean Nusselt number values in Reynolds numbers and the different volume fractions for the Koo & Kleinstreuer model as an example and compared with the Maxwell-Brinkman

Table 4. Average Nusselt number with Richardson number and volume fraction for Koo & Kleinstreuer compared with Maxwell-Brinkman model (as constant properties)

Ri	Nu_{avg}	**φ=**	**φ=0.02**	**φ=0.03**	**φ=0.04**
0.01	Maxwell & Brinkman	14.2212	14.7268	14.9813	15.2375
	Koo & Kleinstreuer	14.2212	17.0254	17.6304	17.8391
	Increase%	0	15.61	17.68	17.07
0.1	Maxwell & Brinkman	9.3241	9.6633	9.8259	9.9889
	Koo & Kleinstreuer	9.3241	11.1571	11.5446	11.6752
	Increase%	0	15.46	17.49	16.88
1	Maxwell & Brinkman	6.366	6.6269	6.7295	6.8318
	Koo & Kleinstreuer	6.366	7.6402	7.8919	7.9694
	Increase%	0	15.29	17.27	16.65
10	Maxwell & Brinkman	5.0398	5.2443	5.3131	5.3803
	Koo & Kleinstreuer	5.0398	6.0289	6.2103	6.2564
	Increase%	0	14.96	16.89	16.28
100	Maxwell & Brinkman	4.4316	4.6196	4.6745	4.7274
	Koo & Kleinstreuer	4.4316	5.3051	5.4568	5.4899
	Increase%	0	14.84	16.74	16.13

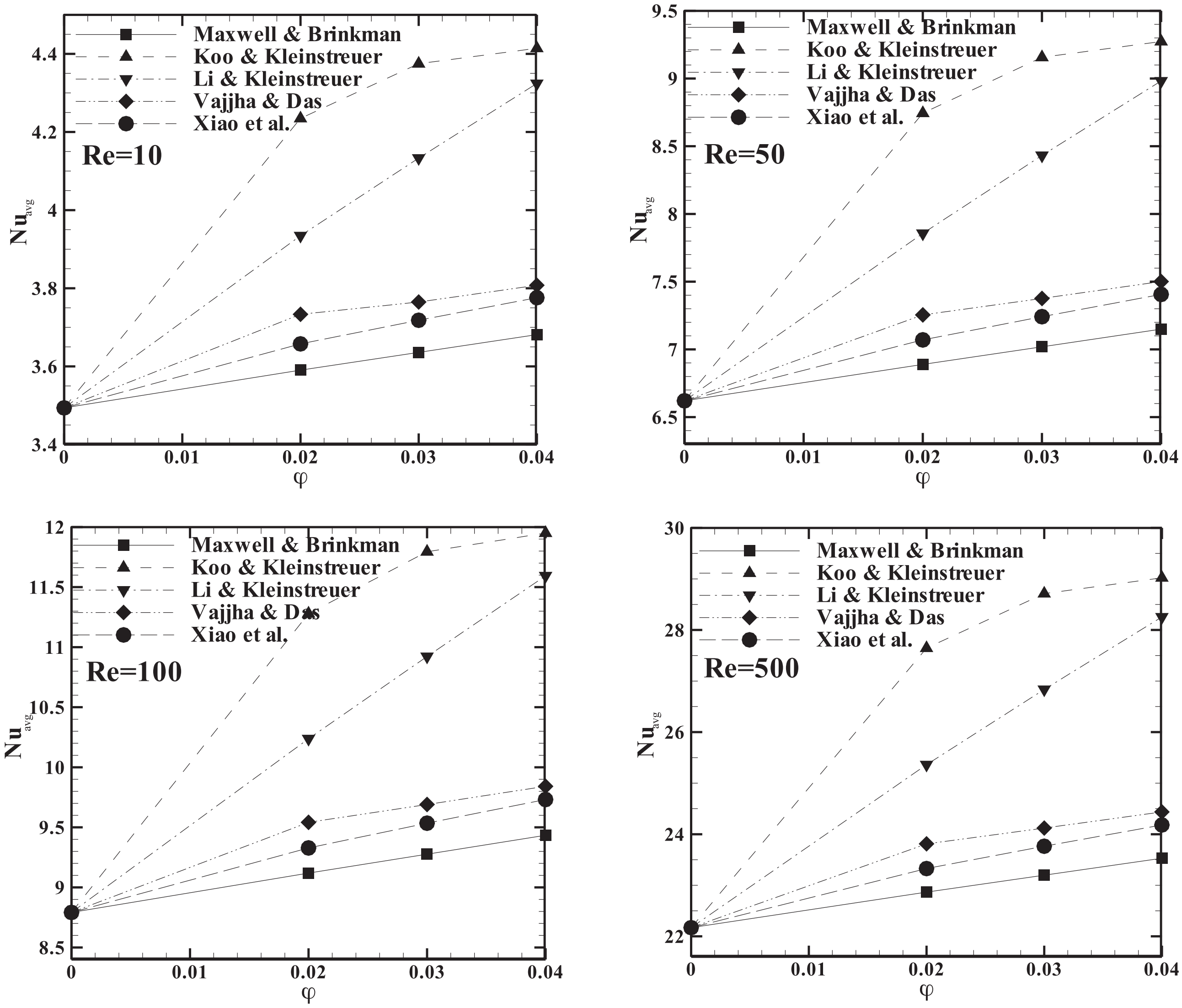

Figure 7. Average Nusselt number with volume fraction employing various thermal conductivity and dynamic viscosity in forced convection.

Table 5. Average Nusselt number with Richardson number and volume fraction for Koo & Kleinstreuer compared with Maxwell-Brinkman model (as constant properties) in forced convection

Re	Nu_{avg}	**0 φ=**	**φ=0.02**	**φ=0.03**	**φ=0.04**
	Maxwell & Brinkman	4.4939	3.5905	3.6359	3.6814
10	Koo & Kleinstreuer	4.4939	4.2347	4.3748	4.4142
	Increase%	0	17.94	20.32	19.91
	Maxwell & Brinkman	6.6206	6.8888	7.0189	7.1497
50	Koo & Kleinstreuer	6.6206	8.7442	9.1566	9.2731
	Increase%	0	26.93	30.46	29.70
	Maxwell & Brinkman	8.7915	9.1193	9.2768	9.4338
100	Koo & Kleinstreuer	8.7915	11.2792	11.7945	11.9500
	Increase%	0	23.68	27.14	26.67
	Maxwell & Brinkman	22.1705	22.8655	23.1981	23.5291
500	Koo & Kleinstreuer	22.1705	27.6448	28.7127	29.0216
	Increase%	0	20.90	23.77	23.34

fixed properties model. In the Koo & Kleinstreuer model, the maximum and lowest increases in the mean Nusselt number, taking into account the effect of Brownian motion relative to the state in which this motion is not considered, are 30.46% (in Reynolds 50 and nanoparticles volume fraction 0.03) and 17.94 %, (in Reynolds 10 and nanoparticles volume fraction 0.02), respectively.

CONCLUSION

In this study, a comprehensive study was performed on the effect of different models of Brownian motion of nanoparticles on increasing the heat transfer of water/aluminum-oxide nanofluids. The study was performed numerically for the square cavity in three modes of natural, mixed, and forced convection by changing the independent parameters such as volume fraction, Rayleigh number, and Richardson number. The following is a summary of the results. 1) In all the studied models and in all cases (natural, mixed and forced convection), the average Nusselt number in the case where the effect of Brownian motion is considered, is more than the case where the effect of this motion is not considered. 2) In natural convection, in all models and in all Rayleigh numbers, the average Nusselt number increases with increasing volume fraction. The Koo & Kleinstreuer and Li & Kleinstreuer models show the largest increase in the Nusselt number with increasing volume fraction. In the Koo & Kleinstreuer model, the maximum and lowest increases in the mean Nusselt number, taking into account the effect of Brownian motion relative to the state in which this motion is not considered, are 23.91% (in Rayleigh 10^3, volume fraction 0.03) and 15.45% (in Rayleigh 10^5, volume fraction is 0.02), respectively. 3) In mixed convection, in all models and in all Richardson numbers, the mean Nusselt number increases with increasing volume fraction. The Koo & Kleinstreuer and Li & Kleinstreuer models show the largest increase in the Nusselt number with increasing volume fraction. In the Koo & Kleinstreuer model, the highest and lowest increases in the mean Nusselt number, taking into account the effect of Brownian motion relative to the state in which this motion is not considered, are 17.68% (in Richardson 0.01, volume fraction 0.03), and is 14.84% (in Richardson 100, volume fraction is 0.02) respectively. 4) In forced convection in all models and in all Reynolds numbers, the average Nusselt number increases with increasing volume fraction. The Koo & Kleinstreuer and Li & Kleinstreuer models show the largest increase in the Nusselt number with increasing volume fraction. In the Koo & Kleinstreuer model, the maximum and lowest increases in the mean Nusselt number, taking into account the effect of Brownian motion relative to the state in which this motion is not considered, are 30.46% (in Reynolds 50, volume fraction 0.03) and is 17.94% (in Reynolds 10, volume fraction is 0.02), respectively.

AUTHORSHIP CONTRIBUTIONS

Authors equally contributed to this work.

DATA AVAILABILITY STATEMENT

The authors confirm that the data that supports the findings of this study are available within the article. Raw data that support the finding of this study are available from the corresponding author, upon reasonable request.

CONFLICT OF INTEREST

The author declared no potential conflicts of interest with respect to the research, authorship, and/or publication of this article.

ETHICS

There are no ethical issues with the publication of this manuscript.

REFERENCE

[1] Pourfattah F, Abbasian Arani AA, Babaie MR, Nguyen HM, Asadi A. On the thermal characteristics of a manifold microchannel heat sink subjected to nanofluid using two-phase flow simulation. Int J Heat Mass Transf 2019;143:118518. [CrossRef]

[2] Abbasian Arani AA, Aberoumand H, Aberoumand S, Moghaddam AJ, Dastanian M. An empirical investigation on thermal characteristics and pressure drop of Ag-oil nanofluid in concentric annular tube. Heat Mass Transf 2016;52:1693–1706. [CrossRef]

[3] Hemmat Esfe M, Abbasian Arani AA, Aghaie A, Wongwises S. Mixed convection flow and heat transfer in an up-driven, inclined, square enclosure subjected to DWCNT-water nanofluid containing three circular heat sources. Curr Nanosci 2017;13:311–323. [CrossRef]

[4] Abbasian Arani AA, Kakoli E, Hajialigol N. Double-diffusive natural convection of Al2O3-water nanofluid in an enclosure with partially active side walls using variable properties. J Mech Sci Technol 2014;28:4681–4691. [CrossRef]

[5] Rajesh V, Mallesh MP, Sridevi Ch. Transient MHD nanofluid flow and heat transfer due to a moving vertical plate with thermal radiation and temperature oscillation effects. Procedia Eng 2015;127:901–908. [CrossRef]

[6] Shahriari A, Jahantigh N, Rakani F. Providing An Analytical Model In Determining Nanofluids. IJE Trans C Aspects 2017;30:1919–1924. [CrossRef]

[7] Sepehrnia M, Khorasanizadeh H, Sadeghi R. Investigation of the nanofluid flow field and simultaneous heat transfer in microchannel thermowells with triangular microchannels and four different arrays. J Mech Eng Univ Amirkabir 2017.

[8] Sepehrnia M, Khorasanizadeh H, Sadeghi R. Three-dimensional study of the effects of two input/output current arrays and the use of nanofluids on the performance of a thermowell with triangular micro-channels. Mech Eng 2016;16:27–38.

[9] Rajesh V, Mallesh MP, Bég OA. Transient MHD free convection flow and heat transfer of nanofluid past an impulsively started vertical porous plate in the presence of viscous dissipation. Procedia Mater Sci 2015;10:80–89. [CrossRef]

[10] Seth GS, Mishra MK. Analysis of transient flow of MHD nanofluid past a non-linear stretching sheet considering. Exp Therm Fluid Sci 2016;72:182–189.

[11] Fan LW, Li JQ, Li DY, Zhang L, Yu ZT, Cen KF. The effect of concentration on transient pool boiling heat transfer of graphene-based aqueous nanofluids. Int J Therm Sci 2015;91:83–95. [CrossRef]

[12] Suganthi KS, Vinodhan VL, Rajan KS. Heat transfer performance and transport properties of ZnO-ethylene glycol and ZnO-ethylene glycol-water nanofluid coolants. Appl Energy 2014;135:548-559. [CrossRef]

[13] Li H, He Y, Hu Y, Jiang B, Huang Y. Thermophysical and natural convection characteristics of ethylene glycol and water mixture based ZnO nanofluids. Int J Heat Mass Transf 2015;91:385-389. [CrossRef]

[14] Goswami KD, Chattopadhyay A, Pandit SK. Brownian motion of magnetonanofluid flow in an undulated partially heated enclosure. Int J Mech Sci 2021;198:106346. [CrossRef]

[15] Harish R, Sivakumar R. Effects of nanoparticle dispersion on turbulent mixed convection flows in cubical enclosure considering Brownian motion and thermophoresis. Powder Technol 2021;378(Part A):303–316. [CrossRef]

[16] Mohammad Tehrani B, Rahbar-Kelishami A. Influence of enhanced mass transfer induced by Brownian motion on supported nanoliquids membrane: Experimental correlation and numerical modelling. Int J Heat Mass Transf 2021;148:119034. [CrossRef]

[17] Goudarzi S, Shekaramiz M, Omidvar A, Golab E, Karimipour A. Nanoparticles migration due to thermophoresis and Brownian motion and its impact on Ag-MgO/Water hybrid nanofluid natural convection. Powder Technol 2020;375:493–503. [CrossRef]

[18] Mittal AS, Patel HR. Influence of thermophoresis and Brownian motion on mixed convection two dimensional MHD Casson fluid flow with non-linear radiation and heat generation. Physica A 2020;537:122710. [CrossRef]

[19] Borzuei M, Baniamerian Z. Role of nanoparticles on critical heat flux in convective boiling of nanofluids: Nanoparticle sedimentation and Brownian motion. Int J Heat Mass Transf 2020;150:119299. [CrossRef]

[20] Dogonchi AS, Seyyedi SM, Hashemi-Tilehnoee M, Chamkha AJ, Ganji DD. Investigation of natural convection of magnetic nanofluid in an enclosure with a porous medium considering Brownian motion. Case Stud Therm Eng 2019;14:100502. [CrossRef]

[21] Mburu ZM, Mondal S, Sibanda P, Sharma R. A Numerical Study of Entropy Generation on an Oldroyd-B Nanofluid flow Past a Riga Plate. J Therm Eng 2021;7:845–866. [CrossRef]

[22] Makkar V, Poply V, Goyal R, Sharma N. Numerical investigation of MHD Casson Nanofluid Flow towards a Non-linear Stretching Sheet in presence of Double-Diffusive effects along with Viscous and Ohmic Dissipation. J Therm Eng 2021;7:1–17. [CrossRef]

[23] Mburu ZM, Mondal S, Sibanda P, Sharma R. A Numerical Study of Entropy Generation on Oldroyd-B Nanofluid Flow Past a Riga Plate. J Therm Eng. 2021;7(4):845–866.er's slip boundary condition. Adv Powder Technol 2017;28(2):375–384. [CrossRef]

[24] Ehteram HR, Abbasian Arani AA, Sheikhzadeh GA, Aghaei A, Malihi AR. The effect of various conductivity and viscosity models considering Brownian motion on nano fluids mixed convection flow and heat transfer, Transport Phenomena in Nano and Micro Scales 2016;4(1):19–28.

[25] Abbasian Arani AA, Mahmoodi M, Sebdani SM. On the Cooling Process of Nanofluid in a Square Enclosure with Linear Temperature Distribution on Left Wall, Journal of Applied Fluid Mechanics 2014;7(4):591–601. [CrossRef]

[26] Abdulvahitoglu A. Using analytic hierarchy process for evaluating different types of nanofluids for engine cooling systems, Thermal Science 2019;23(5) Part B:3199–3208. [CrossRef]

[27] Mahmoodi M, Abbasian Arani AA, Mazrouei Sebdani S, Nazari S, Akbari M. Free convection of a nanofluid in a square cavity with a heat source on the bottom wall and partially cooled from sides, Thermal Science 2014;18(suppl. 2):283–300. [CrossRef]

[28] Abbasian Arani AA, Ababaei A, Sheikhzadeh GA, Aghaei A. Numerical simulation of double-diffusive mixed convection in an enclosure filled with nanofluid using Bejan's heatlines and masslines, Alexandria Engineering Journal 2018;57(3):1287–1300. [CrossRef]

[29] Kilic M, Abdulvahitoglu A. Numerical investigation of heat transfer at a rectangular channel with combined effect of nanofluids and swirling jets in a vehicle radiator, Thermal Science 2019;23(6) Paart A:3627–3637. [CrossRef]

[30] Lyu Z, Pourfattah F, Abbasian Arani AA, Asadi A, Foong LK. On the thermal performance of a fractal microchannel subjected to water and kerosene carbon nanotube nanofluid, Scientific Reports 2020;10(1):1–16. [CrossRef]

[31] Koo J, Kleinstreuer C. A new thermal conductivity model for nanofluids, Journal of Nanoparticle Research 2004;6:577–588. [CrossRef]
[32] Li J, Kleinstreuer C. Thermal performance of nanofluid flow in microchannels, International Journal of Heat and Fluid Flow 2008;29:1221–1232. [CrossRef]
[33] Vajjha RS, Das DK. Experimental determination of thermal conductivity of three nanofluids and development of new correlations, International Journal of Heat and Mass Transfer 2009;52:4675–4682. [CrossRef]
[34] Xiao B, Yang Y, Chen L. Developing a novel form of thermal conductivity of nanofluids with Brownian motion effect by means of fractal geometry, Powder Technology 2013;239:409v414. [CrossRef]
[35] Khanafer K, Vafai K. A critical synthesis of thermophysical characteristics of nanofluids, International Journal of Heat and Mass Transfer 2011;54:4410–4428. [CrossRef]
[36] Abu-Nada E, Masoud Z, Hijazi A. Natural convection heat transfer enhancement in horizontal-concentric annuli using nanofluids, International Communications in Heat and Mass Transfer 2008;35:657–665. [CrossRef]
[37] Aminossadati SM, Ghasemi B. Natural convection of water-CuO nanofluid in a cavity with two pairs of heat source-sink, International Communications in Heat and Mass Transfer 2011;38:672–678. [CrossRef]
[38] Chamkha AJ, Abu-Nada E. Mixed convection flow in single- and double-lid driven square cavities filled with water-Al_2O_3 nanofluid: Effect of viscosity models, European Journal of Mechanics B/Fluids 2012;36:82–96. [CrossRef]